Poisson-Nernst-Planck model of ion current rectification through a nanofluidic diode

Dragoş Constantin* and Zuzanna S. Siwy†
Department of Physics and Astronomy, University of California, Irvine, California 92697, USA
(Received 8 June 2007; revised manuscript received 31 July 2007; published 15 October 2007)

We have investigated ion current rectification properties of a recently prepared bipolar nanofluidic diode. This device is based on a single conically shaped nanopore in a polymer film whose pore walls contain a sharp boundary between positively and negatively charged regions. A semiquantitative model that employs Poisson and Nernst-Planck equations predicts current-voltage curves as well as ionic concentrations and electric potential distributions in this system. We show that under certain conditions the rectification degree, defined as a ratio of currents recorded at the same voltage but opposite polarities, can reach values of over 1000 at a voltage range $\langle -2\ \mathrm{V}, +2\ \mathrm{V}\rangle$. The role of thickness and position of the transition zone on the ion current rectification is discussed as well. We also show that the rectification degree scales with the applied voltage.

DOI: 10.1103/PhysRevE.76.041202 PACS number(s): 66.10.−x, 81.05.Zx, 02.60.Cb, 81.07.De

I. INTRODUCTION

Nanopores in polymer films and silicon materials have attracted a lot of scientific interest due to their application as biomimetic systems for models of biological channels [1–3], and as biosensors [4–7]. Nanopores are also used as a basis for building ionic devices for controlling flow of ions and charged molecules in a solution [8]. In these systems electrostatic and hydrophobic interactions between the ions and molecules that pass through the pore and the pore walls are used to amplify or stop the transport. Our group has recently prepared a nanofluidic diode [9] which rectifies ion current in a similar way as a bipolar semiconductor diode rectifies electron current. This diode is based on a single conically shaped nanopore in a polymer film with openings of several nm and 1 μm, respectively. The surface charge of the pore is patterned so that two regions of the pore with positive and negative surface charges create a sharp barrier called the transition zone. This nanofluidic diode is bipolar in character since both positively and negatively charged ions contribute to the measured current. Another type of nanofluidic diode was prepared in the group of Majumdar and co-workers [10] with a sharp barrier between a positively charged zone and a neutral part of the pore. The presence of only one type of surface charge causes the latter device to be unipolar.

In this paper we provide a semiquantitative description of ion current rectification of the bipolar diode based on single conical nanopores. We use continuum mean-field theory, and more precisely Poisson and Nernst-Planck (PNP) equations, to define our model [11–14] that we apply to describe current-voltage characteristics as well as profiles of ionic concentrations and electric potential in the system. Our model is based on a similar approach as described by Cervera *et al.* in [15,16]. We would like to mention that the model of the nanofluidic diode based on a rectangular channel with limiting length of tens of nanometers presented in [17] combines PNP with Navier-Stokes equations. Nanopores considered here are significantly narrower with the smaller diameter around 5 nm. Therefore, we consider here only PNP equations, because in nanopores of diameters less than 10 nm, electrophoresis is known to be the most dominant process [10,18].

It is important to mention that continuum description of ion transport by the PNP equations has successfully rendered the main properties of many biological channels, e.g., see [19] for the calcium channels treatment. When compared to more precise but computational expensive techniques, e.g., Brownian dynamics [20], the continuum approach has a clear advantage in terms of computing cycles. As discussed in [20] this description produces results which correctly render the physical and chemical phenomena occurring inside a cylindrical nanopore whose diameter is bigger than 2 Debye lengths of the considered ionic species. Hence it is plausible to obtain valid results for the conical nanopores as long as their smallest diameter is bigger than 2 Debye lengths in the examined system. It is also important to mention that transport properties of nanopores of such dimensions are not influenced by induced charges that are created on the pore walls of the polymeric membrane. We indeed have a sharp barrier between a water solution of dielectric constant 80, and the polymer membrane characterized by the dielectric constant of about 3. As discussed in [21,22], the effect of the induced charge forces in nanopores of diameter larger than 2 nm can be neglected.

In this study, we thoroughly discuss how ion current rectification in a nanofluidic diode depends on the position of the transition zone between the two regions of the pore walls with opposite surface charges. Influence of the width of the transition zone on rectifying properties of the device is studied in detail as well. We identify the range of values for the position of the transition zone and its width that lead to a significant enhancement of the current rectification degree. This aspect is of crucial importance for further improvement of these new devices. The paper is organized as follows. In Sec. II we explain the experimental system and present the theoretical basis of our model. In Sec. III we present the results of the analysis and provide directions to future improvements of the design of nanofluidic diodes. Section IV compares results obtained from the full two-dimensional PNP model and its one-dimensional approximation that we used in this paper.

*dragos@uci.edu
†zsiwy@uci.edu

 ©2007 The American Physical Society

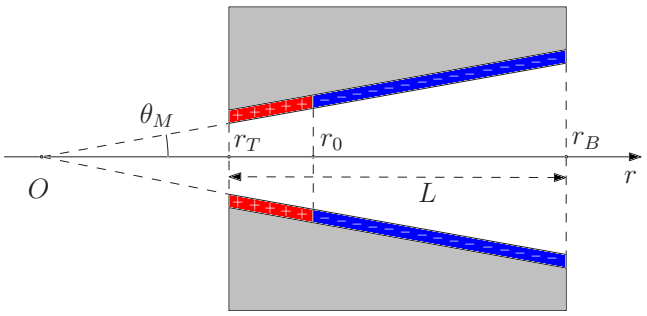

FIG. 1. (Color online) Pore geometry with schematic representation of surface charge distribution creating a bipolar nanofluidic diode.

II. METHODS

In this section we present the experimental results and the theoretical background which provide the basis of our simulations. In Sec. II A we briefly explain the experimental facts which inspired the current project. Sections II B–II D are devoted to the theoretical background.

A. Experiment

Single nanopores in polymer (polyethylene terephthalate, in short PET) film were prepared by the track-etching technique as described in [23,24]. Briefly, the method consists of irradiation of polymer films with single swift heavy ions [25] (Gesellschaft fuer Schwerionenforschung, Darmstadt, Germany), and subsequent asymmetric etching of the irradiated foils with 9*M* NaOH [23]. This procedure leads to preparation of membranes that contain only one pore with the small opening, called tip, as narrow as several nanometers in diameter, and the big opening, called base, with micrometer size diameter. As the result of the chemical etching, there are carboxyl groups formed on the surface of the pore walls with density of about one per nm^2. The carboxyl groups therefore determine the surface charge density to -0.16 C/m^2 [26]. In order to modify the surface of PET nanopores we used the method of coupling carboxyl and amine groups with 1-ethyl-3-[3-dimethylaminopropyl]-carbodiimide hydrochloride (EDC) [27]. The reaction between the carboxyl groups and diamines changes the surface charge from negative to positive. Targeted modification of the tip was obtained by introducing the reagent mixture only on the side of the membrane with the small opening [9]. The other side of the membrane was in contact with a buffer solution. A conical shape of the pore makes the distribution of the diamines and EDC in the pore extremely nonhomogeneous. There is a high concentration of the reagents at the tip of the pore that assures the chemical modification reaction of the tip to occur [9]. The concentration of diamines and EDC at the remaining part of the pore is very low, therefore, this part remains negatively charged. As the result, we obtain a surface charge distribution as schematically shown in Fig. 1. An example of the current-voltage characteristic through such a device recorded at 0.1*M* KCl and *p*H 5.5 is presented in Fig. 2. The rectification degree of the system is defined as the ratio of currents recorded for positive and negative voltages, respectively,

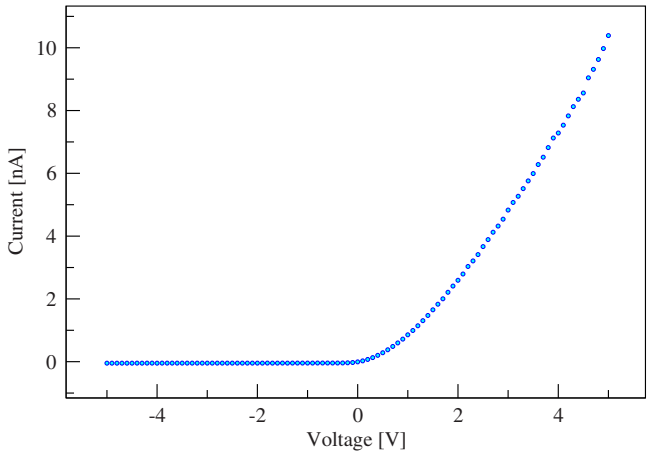

FIG. 2. (Color online) Experimental data of ion current recorded at 0.1*M* KCl, *p*H 5.5 through a single conical nanopore with surface charge distribution as shown in Fig. 1 [9]. The pore diameters were 5 nm and 1000 nm, respectively.

$$f(V) = \frac{|I(V)|}{|I(-V)|}. \tag{1}$$

The rectification degree of this system (Fig. 2) equals 217 at 5 V [9]. We would like to mention that even devices with uniform surface charge distribution rectify the current but their rectification degree is one order of magnitude smaller than the one obtained for the systems described above [2,23]. It is also important to mention that the single pore diode is a nanorealization of bipolar membranes consisting of cationic and anionic membranes [28–30].

B. Modeling

Before we start to introduce the theoretical basis of the model we would like to specify the notation. We have assigned the subscripts "*T*" and "*B*" to designate the various physical quantities computed at the tip and at the base sides of the pore, respectively. In this sense r_T is the location of the pore tip and r_B is the location of the pore base (Fig. 1). The thickness of the membrane is denoted with *L*. The cone opening angle is θ_M. The membrane is immersed in an electrolyte containing potassium and chloride ions, and in addition we apply an external electric field with the help of two electrodes positioned far away from the membrane on each side of the pore. Due to $G\Omega$ resistance of single nanopores, the voltage drop will occur only inside the pore, not in the electrolyte bulk. By convention, we will keep the electrode on the pore tip side grounded such that the sign of the electric potential difference will be controlled by the electrode on the base side of the pore. The existence of the external field causes the ions to migrate toward the electrodes, which we record as ion current. We would like to mention that for small pores [2] and more complex electrolytes in which chemical reactions can occur, one observes large fluctuations of ion current in time [31,32]. However our model in its present form does not include chemical reactions between components of the electrolyte, and therefore the system will

reach a stationary regime, i.e., the ionic fluxes are constant in time. In nanofluidic diodes, constant currents at constant voltages are indeed observed experimentally. Our goal is to compute the steady state current for a fixed set of physical and chemical parameters. Hence, we express the stationarity of the ionic fluxes using the Nernst-Planck condition. To be more specific we assume that for each ionic species, indexed by "i," the molar flux defined as

$$\vec{J}_i(\vec{r}) = -D_i[\nabla c_i(\vec{r}) + z_i c_i(\vec{r})\nabla\,\phi(\vec{r})] \tag{2}$$

is conserved, i.e., it obeys the Nernst-Planck condition

$$\nabla \vec{J}_i(\vec{r}) = 0, \tag{3}$$

where D_i is the diffusion coefficient of an ion i, c_i is the molar concentration, and z_i is the charge number of the ion i. We have denoted with ϕ the total electric potential in RT/F units, which satisfies the Poisson equation

$$\Delta\phi(\vec{r}) = -\frac{F^2}{\varepsilon RT}\left(\sum_i z_i c_i(\vec{r}) + \frac{1}{rF}\delta(\theta-\theta_M)\sigma(r)\right), \tag{4}$$

where ε is the electric permittivity of the medium and the summation is carried over all the ions present in the solution. The parameter F is the Faraday constant, R is the gas constant, and $T=293.15$ K is the absolute temperature. The polar angle θ_M which appears in the Dirac distribution represents the cone angle (see Fig. 1). The PNP Eqs. (3) and (4) provide a complete set of equations which together with appropriate boundary conditions allow us to determine the concentration of each ionic species and the electric potential inside the pore. Consequently, the total ion current density along an arbitrary direction $\hat{n}$ can be computed with the help of (2),

$$j_n(\vec{r}) = F\sum_i z_i \vec{J}_i(\vec{r})\cdot\hat{n}, \tag{5}$$

where the summation is performed again over all considered ions.

As the problem has azimuthal symmetry with respect to the pore axis, it gets reduced to a set of two-dimensional (2D) second-order partial differential equations. To simplify the problem even more we perform an analytical integration with respect to the polar angle and we obtain a set of second-order ordinary differential equations which is finally solved numerically. We would like to mention that after integration one must neglect one term in order to obtain a well-defined set of ordinary differential equations [16]. Also we assume that the polar component in Eq. (3) is negligible. Our comparison tests performed in Sec. IV between the full two-dimensional problem and the approximated one-dimensional (1D) treatment show insignificant differences in both the quantitative and the qualitative results. Hence the solution of the problem will provide averaged quantities in the sense that the polar angle dependence is lost during the integration. However, our main interest is to compute the ion current, which involves averaging along the polar coordinate, therefore we do not lose any information. To be more specific, the differential equations which result from the above-described procedure have the following structure:

$$\frac{d}{dr}\left[r^2\left(\frac{dc_i(r)}{dr} + z_i c_i(r)\frac{d\phi(r)}{dr}\right)\right] = 0 \quad \forall\, i \tag{6}$$

and

$$\frac{1}{r^2}\frac{d}{dr}\left(r^2\frac{d\phi(r)}{dr}\right) = -\frac{F^2}{\varepsilon RT}\left(\sum_i z_i c_i(r) + X(r)\right), \tag{7}$$

where the quantities $c_i(r)$ and $\phi(r)$ in Eqs. (6) and (7) come from integration, i.e.,

$$\phi(r) = \frac{1}{1-\cos\,\theta_M}\int_0^{\theta_M} d\theta\,\sin\,\theta\phi(r,\theta), \tag{8a}$$

$$c_i(r) = \frac{1}{1-\cos\,\theta_M}\int_0^{\theta_M} d\theta\,\sin\,\theta c_i(r,\theta), \tag{8b}$$

and the function $X(r)$ is given by

$$X(r) = \frac{\sin\,\theta_M\sigma(r)}{Fr(1-\cos\,\theta_M)}, \tag{9}$$

where $\sigma(r)$ represents the surface charge density. For simplicity we have kept the same notation for the averaged quantities $c_i(r)$ and $\phi(r)$. We will use the functional dependence on the polar angle to distinguish between the averaged quantities $c_i(r)$ and $\phi(r)$, and the nonaveraged quantities $c_i(r,\theta)$ and $\phi(r,\theta)$.

C. Boundary conditions

To completely define the problem we must specify the boundary conditions. These conditions are derived from the so-called Donnan equilibrium conditions which express the thermodynamic equilibrium between the membrane with excess surface charge and the ionic concentrations in the bulk. One can derive these conditions as in [33] and obtain the following relations for the concentrations at the pore border:

$$c_i(r_j) = c_{0i}\exp[-z_i\phi_D(r_j)], \tag{10}$$

where c_{0i} represents the bulk concentration of ion i and $j=T,B$ indexes the tip and the base sides of the pore, respectively. ϕ_D is the Donnan potential defined as the potential difference created across an ion exchange membrane,

$$\phi_D(r_j) = \phi(r_j) - \phi_j, \tag{11}$$

where ϕ_j is the electric potential at the corresponding electrode. The electroneutrality condition, which has the form

$$\sum_i z_i c_i(r_j) + X(r_j) = 0, \tag{12}$$

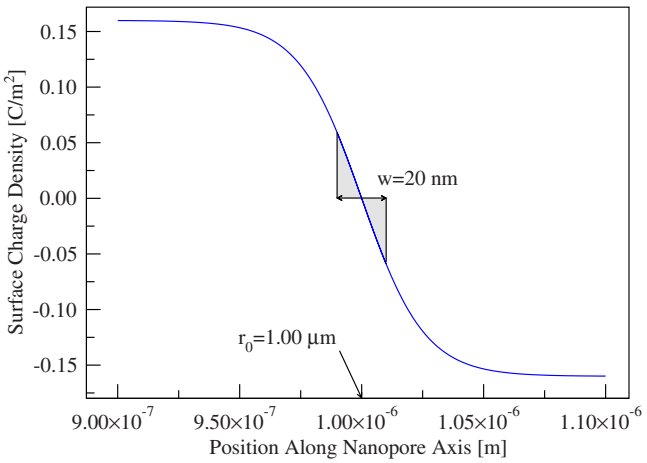

FIG. 3. (Color online) Surface charge distribution that has been used in calculations. The width of the transition zone w and position of the zero charge point r_0 are indicated in the figure.

provides an equation for $\exp[\phi_D(r_j)]$. Hence, the boundary conditions can be derived from (10) and (12) as

$$c_i(r_j) = \frac{1}{2}[-z_i X(r_j) + \sqrt{X(r_j)^2 + 4c_0^2}], \tag{13}$$

and

$$\phi(r_j) = \phi_j - \frac{1}{z_i}\ln\frac{c_i(r_j)}{c_0}. \tag{14}$$

The PNP equations (6) and (7) together with the boundary conditions (13) and (14) form the base of our model. We deal with two ionic species in our system, i.e., K^+ and Cl^-, therefore we must solve a set of three second-order ordinary differential equations.

D. Surface charge distribution

The charge distribution is formed by two distinct regions with positive and negative surface charges, respectively, and a transition zone between them. These regions are characterized by the asymptotic values of the surface charge density, i.e., the value of σ far away from the transition zone. We employ some simplifying assumptions in order to characterize the surface charge distribution in the transition zone. First, we consider that the magnitudes of the asymptotic values of the positive and negative surface charge densities are the same and equal to e_0/nm^2, where e_0 is the elementary charge. Additionally, we assume that the transition between the positive and negative charges on the pore walls is made in a symmetric, continuous, and monotonic way. Hence, we will consider the surface charge density in the pore to be described by the logistic-type function (see Fig. 3),

$$\sigma(r) = \sigma_0\left(-1 + \frac{2}{1+\exp[-2k(r-r_0)]}\right), \tag{15}$$

where $\sigma_0 = -e_0/\mathrm{nm}^2$, r_0 is the position along the pore axis where $\sigma(r)$ equals zero, and k measures the slope of σ in the transition zone. Another equivalent way to characterize the charge distribution in the transition zone is to specify the transition zone width w (see Fig. 3) which is defined as the part of the pore where the magnitude of the charge is below $|\sigma_0|/e$, i.e.,

$$w = \frac{1}{2k}\ln\frac{m_2}{m_1}, \tag{16}$$

where $m_{1,2} = \tanh^{+1}(1/2)$ are constants. In this problem there are many parameters which can be modified. However our main interest was to see how the properties of the nanofluidic diode modify when the surface charge distribution parameters change. Therefore, we have chosen to keep all the parameters constant, the only exception being r_0 and w, the parameters, which we believe can be controlled experimentally.

III. RESULTS

As we have discussed in the preceding section we must solve a boundary value problem (BVP) defined by a set of three second-order ordinary differential equations. The solution will provide the potassium and chloride concentrations and the electric potential as functions of the coordinate along the pore axis. We have used the BVP solver described in [34] to compute the solution with an error less than 10^{-6}. The solution of the computation is used to evaluate the ion current which is given by

$$I = 2\pi(1-\cos\theta_m)r^2 j_r(r), \tag{17}$$

where j_r is the radial component of the ion current density given by (5). As we expect the current is not dependent on the radial coordinate and it has a constant value along the pore axis.

A. Current-voltage curves and ionic concentration profiles

The system that we have considered is a single conical nanopore with pore diameters 5 nm and 1000 nm, respectively, at symmetric electrolyte conditions of 100 mM KCl on both sides of the membrane. We have used a relative dielectric constant value of $\epsilon_r = 80$ and we have considered a constant value for the diffusion coefficients throughout the volume of the pore, i.e., $D_{\mathrm{Cl}} = 2.03 \times 10^{-9}$ m^2/s and $D_{\mathrm{K}} = 1.95 \times 10^{-9}$ m^2/s [16]. The thickness of the membrane is 12 μm. Figures 4(a)–4(c) show the numerical solutions of the corresponding distributions of potassium and chloride ionic concentrations in forward and reverse bias, respectively. Figure 4(d) presents the distribution of the electric potential in the nanopore for various applied voltages. The increase of the ionic concentrations in the forward bias is remarkable. Concentrations of both ions, potassium and chloride, have increased by an order of magnitude, compared to the bulk concentration of 100 mM. This result also confirms bipolar character of our device, since K^+ and Cl^- contribute almost equally to the measured ion current. Ionic concentrations at the reverse bias are dramatically different. We see significantly lower concentrations of both ions in a region close to the transition zone which indicates the formation of the depletion zone. The inset in Fig. 4(c) shows a

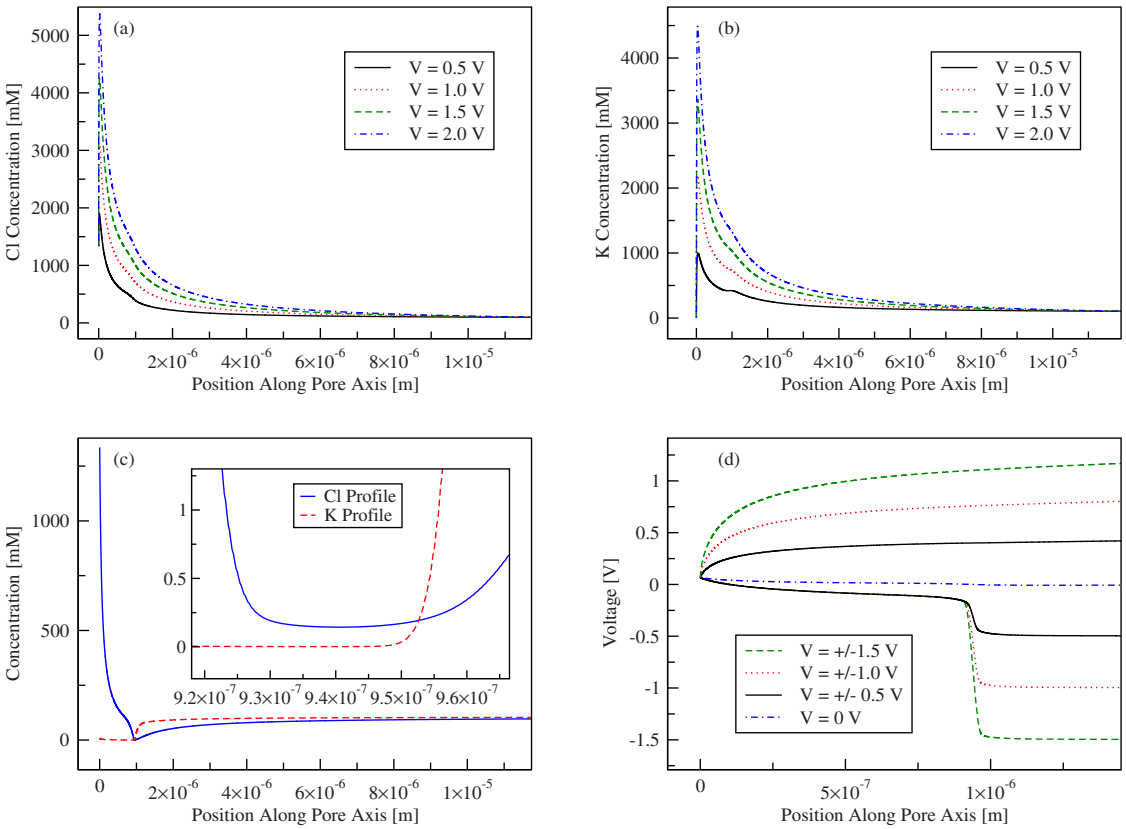

FIG. 4. (Color online) Profiles of ionic concentrations and electric potential in a nanofluidic diode based on a single conical nanopore for $r_0=1$ μm, $w=100$ nm, and various voltages as indicated. (a) Profiles of Cl^- concentration in a nanopore for forward bias (positive voltages), (b) K^+ concentration profiles for forward bias, (c) profiles of Cl^- and K^+ concentrations for reverse bias at -1 V, (d) electric potential profiles in the nanopore for forward and reverse bias. The position 0 corresponds to r_T in Fig. 1.

magnified view of the depletion zone where the concentration of both ions drops practically to zero. Figure 4(d) shows profiles of electric potential in the pore for various voltages applied in the forward and reverse directions. Similar to the results for diodes based on rectangular channels and bipolar membranes [10,18,29,30], in our bipolar diode based on single conical nanopores, the whole voltage drop for negative voltages occurs in the depletion zone. This sudden drop of the electric potential causes the appearance of a huge electric field located in the depletion zone, which will effectively block the ionic currents in the reverse bias.

Using the numerical solution and Eq. (17) we compute the ion current. Figure 5 shows a typical current-voltage curve calculated for this nanopore with parameters $r_0=100$ nm and $w=100$ nm. Similar to the experimental data shown in Fig. 2, the model predicts very high rectification degrees with very small ion currents for reverse bias.

B. Position of the depletion zone, dynamics of nanofluidic diode formation

The process of preparation of the nanofluidic diode is based on a chemical reaction of the reagent with the carboxyls groups on the pore walls. This causes change of the position r_0 and increase of the rectification degree in time when the chemical reaction progresses [9]. We decided to investigate in more detail how sensitive the rectification degree is on the position of the transition zone in the pore. Therefore, we numerically performed the experiment of chemical modification of the pore walls. However, the reader must be aware that our surface charge distribution is not

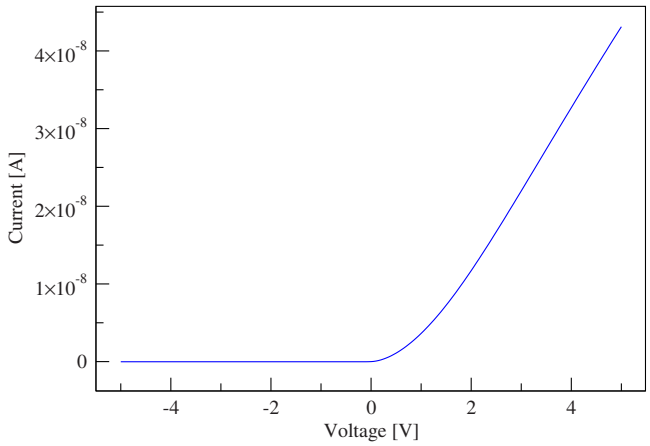

FIG. 5. (Color online) Current-voltage curve for a nanofluidic diode calculated with Eq. (17) for $r_0=100$ nm and $w=100$ nm. The surface charge was assumed as shown in Fig. 3. The pore openings were 5 nm and 1000 nm, respectively.

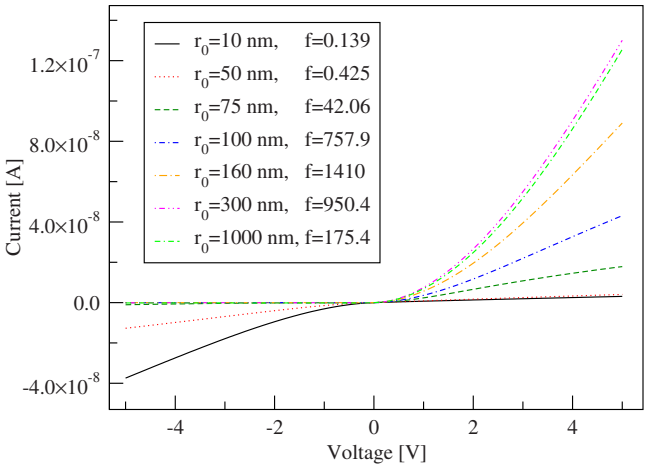

FIG. 6. (Color online) Current-voltage curves for a nanofluidic diode (Fig. 1) for various values of the r_0 parameter when $w = 100$ nm. Note the change of the direction of ion current rectification. The rectification degree, f, was computed at 2 V.

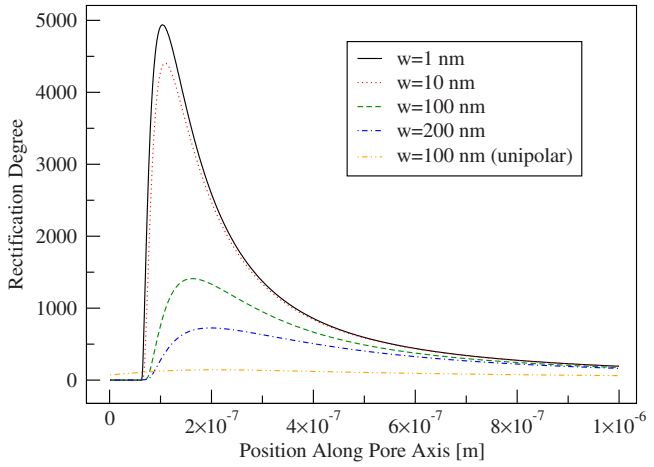

FIG. 7. (Color online) Rectification degree of a nanofluidic diode as a function of r_0 parameter for various thicknesses of the transition zone w (Fig. 3), at 2 V.

necessarily the distribution which corresponds to the real, i.e., experimental, case. In the real case, the shape of $\sigma(r)$ changes in time [9], i.e., it changes with r_0. In our theoretical model, the time evolution is simply described by a translation of $\sigma(r)$ along the radial coordinate. We think, however, that the main features of the experimental charge distribution are present in our model system and this gives us the possibility to get insight into the nanofluidic diode behavior when the surface charge gets modified.

A given value of the transition zone width w was assumed and the position r_0 was moved between the pore tip and its base. In other words, we start from the situation where the whole surface of the pore is negatively charged and finish in a state where the whole surface is positively charged. In the initial and final states we have a homogeneously charged conical geometry that leads to ion current rectification via rocking ratchet mechanism described earlier in [35,36]. The rectification degree was defined in Eq. (1) as the ratio of currents recorded for positive voltages divided by currents recorded for negative voltages. These homogeneously charged conical nanopores are characterized by rectification degrees less than 10. As we move the position r_0 inside the pore the surface charge in the tip changes acquiring more positive charges. As shown in Fig. 6, it is remarkable that a small amount of positive charge in the tip of the pore reverses the direction of rectification and changes the devices from monopolar to bipolar. The rectification degree versus r_0 is shown in Fig. 7 for several values of the transition zone width. The rectification degree increases steeply as we move r_0 inside the pore along its axis, reaches a maximum, and decreases to a value lower than 10, when r_0 is located at the base of the pore. A very strong dependence of the rectification degree on r_0, when r_0 is located at the narrowest part of the pore, suggests that transport properties of the system are determined by the physical and chemical properties of the tip of the nanopore, in this case the surface charge distribution.

Comparison of Figs. 6 and 7 leads to another interesting observation on the relation between the position of the transition zone, the rectification degree, and the values of the ion current. Figure 6 predicts recording very high currents for the forward bias for diodes whose transition zone is located between 300 nm and 1000 nm from the tip. These diodes, however, are characterized by smaller rectification degrees compared to the diodes with r_0 at about 200 nm. In order to understand the relation between the degree of rectification and the current values, we additionally plotted the forward and reverse currents as a function of r_0. As can be seen from Fig. 8, the maximum forward currents are observed for r_0 between 300 nm and 400 nm, while the maximum rectification degree occurs for r_0 around 200 nm. It is because for r_0 between 300 nm and 400 nm the off currents increase as well, leading to an overall smaller rectification degree. Depending on the specifics of the various applications nanofluidic diodes can therefore provide higher (lower) currents and lower (higher) rectification degrees. We would like to emphasize that all of these various properties can be obtained

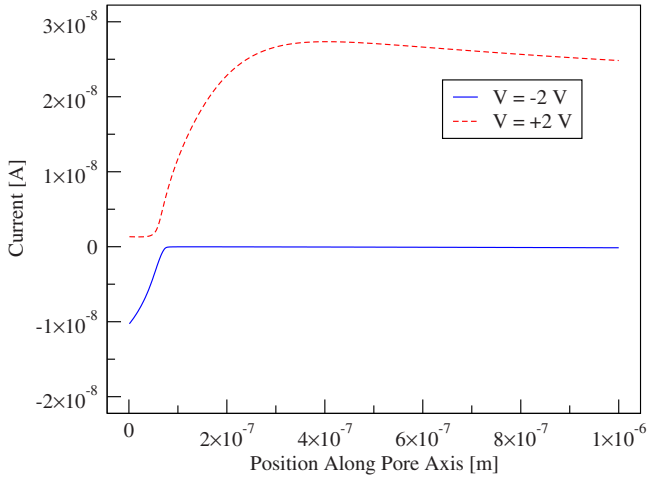

FIG. 8. (Color online) Dependence of the forward and reverse bias currents at $V = \pm 2$ V as functions of the r_0 parameter. The transition width in this case is $w = 100$ nm.

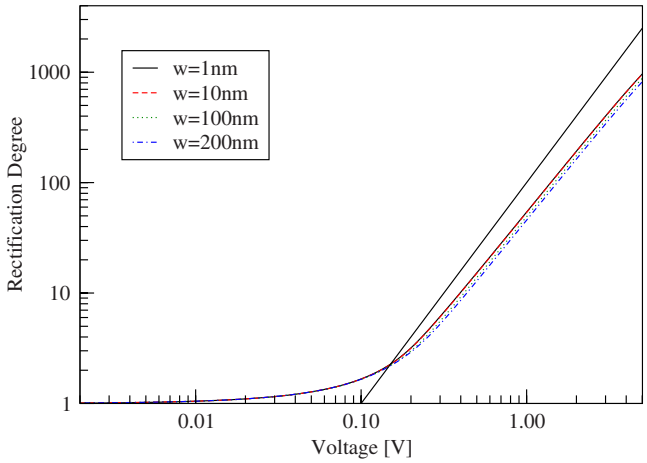

FIG. 9. (Color online) Log-log plot of the rectification degree of a nanofluidic diode (Fig. 1) as a function of applied voltage at $r_0 = 1$ μm and for various values of the w parameter. The straight line is a power law with exponent equal to 2.

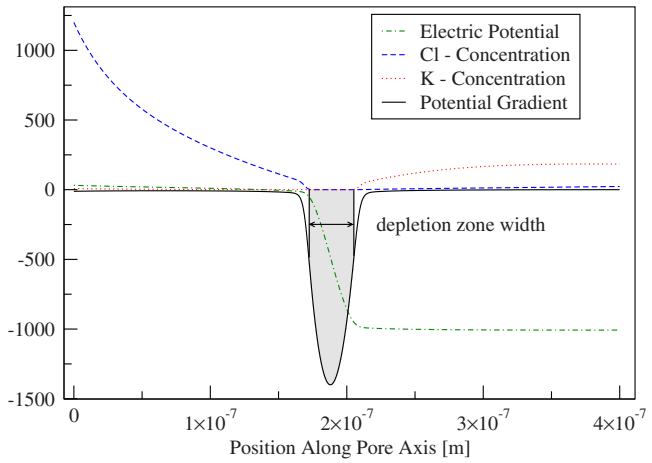

FIG. 10. (Color online) Profiles of ionic concentrations, electric potential, and its first derivative at the depletion zone created at the reverse bias of −2 V. Values have been scaled (see text) to make the graphic visualization possible.

by just changing the position of the zero surface charge point.

As a comparison, we have also included rectification data for a monopolar diode designed such that the tip of the pore was positively charged (0.16 C/m^2) with the rest of the pore neutral (0 C/m^2). The surface charge distribution is similar to the one shown in Fig. 3, the only difference is that r_0 represents in this case the position where the surface charge is one-half its maximum value. The parameter w was set to 100 nm. One can see that overall the rectification degrees for the monopolar diode are much smaller than in case of the bipolar diode when both devices are studied in the same KCl concentration.

Our results show that a huge increase of ion current rectification degrees is possible when the surface of a pore is patterned such that a part of the pore with negative surface charge is brought into contact with a part of the pore with positive surface charge. Our analysis also points to the importance of future experimental efforts aimed at a better control over the width and the position of the transition zone.

C. Scaling of the rectification degree with voltage

We have also analyzed the behavior of the rectification degree with voltage. In Fig. 9 we show the rectification degree of a nanofluidic diode $f(V)$ as a function of voltage ranging between −5 V and +5 V for the case when the transition zone is located 1 μm away from the tip, and for various values of w. We find that $f(V)$ has a power-law dependence for voltages larger than ≈0.3 V,

$$f(V) \propto V^{\gamma}, \tag{18}$$

where the scaling exponent $\gamma \approx 1.81$. For guidance, the power law with exponent equal to 2 is shown in Fig. 9. The power-law scaling of the rectification degree with voltage might suggest the existence of universal scaling. The applicability of the universal scaling and universal scaling exponents to nanofluidic diodes will be investigated in our future studies.

D. Dependence of the depletion zone width on voltage

Another interesting question to consider is the dependence of the depletion zone width w_d on the reverse bias voltages. The depletion zone is defined as the region where mobile charges are absent or at least their number is small compared to the adjacent regions (Fig. 4). This ion-free region appears only in the reverse bias regime. The lack of ions in this zone produces a drop of the electric potential, or in other words, the electric field in this region is strong enough to block the migration of mobile charges through the pore. To help visualize the above statements we have superimposed in Fig. 10 the concentration profiles, the electric potential, and its first derivative which is proportional to the electric field. Since the voltage drops over a very small distance the electric fields created are of the order of magnitude 10^8 V/m. As we have explained above, the electric field has a strong peak in the depletion zone and we have considered the width of this peak to provide the definition for the width of the depletion zone. In order to plot all these profiles in one figure, scaling of their values was necessary. The electric potential was scaled up 50 times and its first derivative was scaled down 5000 times such that all the graphs will provide sufficient details. The plots in Fig. 10 correspond to $w = 100$ nm, $r_0 = 250$ nm, and for a reverse bias voltage of −2 V.

We would like to emphasize the difference between the width of the transition zone w and the width of the depletion zone. Larger w values lead to larger values of w_d, as shown in Fig. 11. For w equal to 1 nm and 10 nm, the resulting w_d for 5 V exceeds the value of the transition zone width that assured formation of much smaller leakage currents, and consequently higher rectification degrees. For the transition zone of width 100 nm and 200 nm, the depletion zone is narrower than the values of w. Larger w_d therefore does not

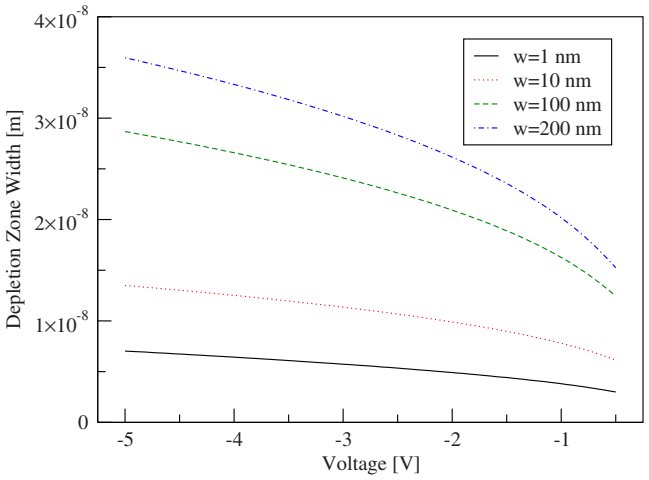

FIG. 11. (Color online) Dependence of depletion zone width w_d on voltage for various values of the width of the transition zone w.

necessarily imply higher rectification degrees, as explained in the preceding section. Smaller values of w and w_d assure larger electric fields for the reverse bias, which also helps formation of a depletion zone of a larger resistance.

IV. COMPARISON BETWEEN 1D MODEL AND 2D PNP MODEL

In this section we present a side-by-side comparison of the results obtained with the procedure described in the first part of the paper and the results obtained from a full treatment of the PNP equations (3) and (4). We will refer to the first set of solutions as the 1D data because the PNP equations (6) and (7) in this case depend only on the radial coordinate. We will refer to the latter set of solutions as the 2D data because the original three-dimensional PNP equations have azimuthal symmetry, hence we must solve a two-dimensional problem.

The 2D solution was obtained using COMSOL Multiphysics™ in conjunction with MATLAB™ on a workstation powered by a 64-bit version of Red Hat Linux™. The solutions have been computed with an error less than 10^{-6}. Similarly to the 1D approach, we have eliminated the bulk by imposing the Donnan equilibrium conditions at the base and the tip of the a nanopore. In order to compare the results, we have performed a similar averaging of the 2D solution as shown in Eq. (8a) and (8b). We have plotted in Fig. 12 the averaged solutions coming from the 2D PNP model and the ones from the 1D model. As one can see, no significant difference was found in the concentration and potential profiles

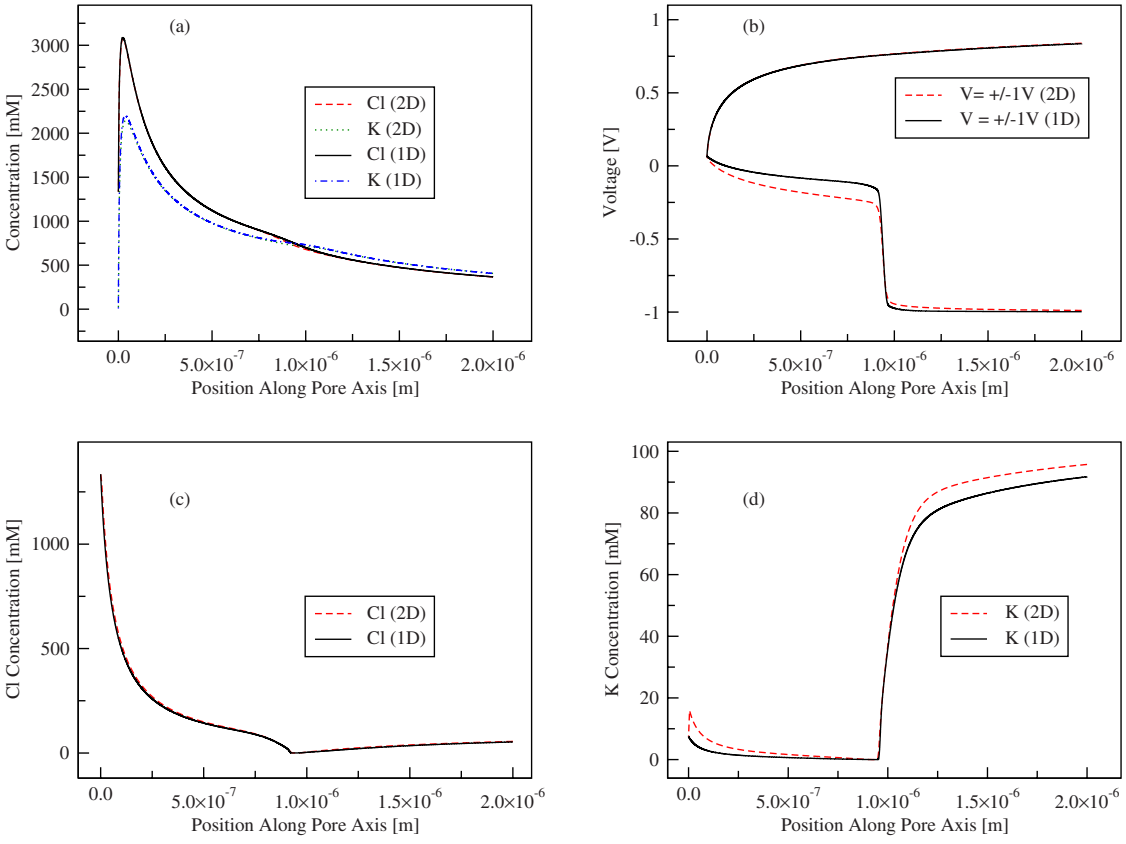

FIG. 12. (Color online) Comparison of the solutions obtained from the 1D and 2D models. Profiles of ionic concentrations and electric potential in a nanofluidic diode based on a single conical nanopore for $r_0=1$ μm, $w=100$ nm. (a) Profiles of Cl^- and K+ concentrations in a nanopore for forward bias at $V=1$ V, (b) electric potential profiles in the nanopore for forward and reverse bias at $V=\pm 1$ V, (c) profiles of Cl^- concentrations for reverse bias at -1 V, (d) K^+ concentration profiles for reverse bias at -1 V.

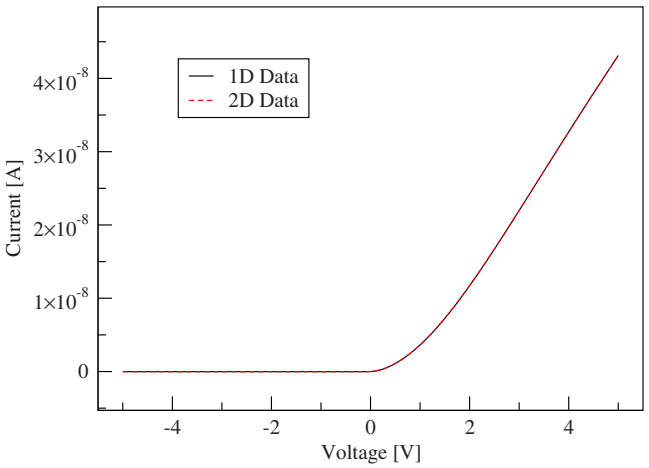

FIG. 13. (Color online) Comparison of the solutions obtained from the 1D and 2D models. Current-voltage curves for a nanofluidic diode calculated with Eq. (17) for $r_0=100$ nm and $w=100$ nm. The surface charge was assumed as shown in Fig. 3. The pore openings were 5 nm and 1000 nm, respectively.

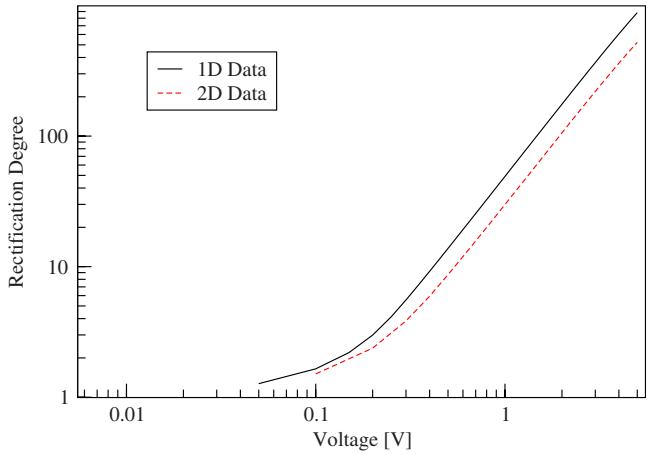

FIG. 14. (Color online) Comparison of the solutions obtained from the 1D and 2D models. Log-log plot of the rectification degree of a nanofluidic diode (Fig. 1) as a function of applied voltage at $r_0=1$ μm and $w=100$ nm parameters.

obtained by the two approaches. Ion currents for the considered set of parameters predicted by the 1D and 2D models differ by no more than several tens of pA (see Fig. 13). We have also checked that the difference between the ion currents for other values of r_0 stays below 1% of the current value. The scaling of ion current rectification degree with voltage (Fig. 14) calculated by the two modeling approaches is also practically the same. The scaling coefficients for the two cases are $\gamma_{1D}=1.81$ and $\gamma_{2D}=1.79$.

We also would like to mention that the 1D computation is at least 500 times faster than the 2D computation. Also the simulations can be performed on any desktop computer in the 1D case whereas the 2D case is quite demanding in terms of computing resources.

V. CONCLUSIONS

The modeling of a nanofluidic diode presented in this paper has been motivated and inspired by a recent experimental realization of this device [9]. In this paper we have shown that rectification degrees of 10^3 can be achieved with this device upon more precise surface charge control. We have shown that the width and the position of the transition zone are parameters which influence very strongly the rectification properties of nanofluidic diodes. These parameters in turn could be controlled by chemical modification of the pore walls. In our studies, as a template for the nanofluidic diode we chose a conical geometry, because patterning of the surface charge of conical pores is well understood [9]. Different widths of the transition zone could be, for example, obtained by changing the opening angle of conical nanopores. Our modeling also provides directions for the future design of the nanofluidic diode in order to prepare versatile devices which meet the requirements of various applications. We have also shown that the results obtained with the 1D model are practically the same as the results obtained with the 2D model.

It would be very interesting to see how the rectification behaves when other parameters of the problem are changed, for example, shape of the nanopore, and magnitude of surface charge. Another interesting aspect of the bipolar diode is the power-law dependence of rectification degrees on voltage, which might suggest existence of universal scaling and critical exponents in the system. Our future studies will be directed toward identification of these critical exponents and relating them to formation of the depletion zone.

ACKNOWLEDGMENTS

The authors thank the Alfred P. Sloan Foundation and the Institute for Complex Adaptive Matter for financial support. The authors are grateful to Dr. Ivan Vlassiouk for stimulating discussions, and Dr. Magdalena Constantin for the careful reading of our paper.

[1] A. A. Lev, Y. E. Korchev, T. K. Rostovtseva, C. L. Bashford, D. T. Edmonds, and C. A. Pasternak, Proc. R. Soc. London **252**, 187 (1993).

[2] Z. Siwy, P. Apel, D. Baur, D. D. Dobrev, Y. E. Korchev, R. Neumann, R. Spohr, C. Trautmann, and K.-O. Voss, Surf. Sci. **532–535**, 1061 (2003).

[3] P. Chen, T. Mitsui, D. B. Farmer, J. Golovchenko, R. G. Gordon, and D. Branton, Nano Lett. **4**, 1333 (2004).

[4] J. Li, D. Stein, C. McMullan, D. Branton, M. J. Aziz, and J. A. Golovchenko, Nature (London) **412**, 166 (2001).

[5] C. Dekker, Nat. Nanotechnol. **2**, 209 (2007).

[6] C. C. Harrell, Y. Choi, L. P. Horne, L. A. Baker, Z. S. Siwy,

and C. R. Martin, Langmuir **22**, 10837 (2006).
[7] A. Mara, Z. Siwy, C. Trautmann, J. Wan, and F. Kamme, Nano Lett. **4**, 497 (2004).
[8] M. A. M. Gijs, Nat. Nanotechnol. **2**, 268 (2007).
[9] I. Vlassiouk and Z. S. Siwy, Nano Lett. **7**, 552 (2007).
[10] R. Karnik, C. Duan, K. Castelino, H. Daiguji, and A. Majumdar, Nano Lett. **7**, 547 (2007).
[11] Z. Schuss, B. Nadler, and R. S. Eisenberg, Phys. Rev. E **64**, 036116 (2001).
[12] B. Nadler, Z. Schuss, A. Singer, and R. S. Eisenberg, J. Phys.: Condens. Matter **16**, S2153 (2004).
[13] D. Chen, J. Lear, and R. S. Eisenberg, Biophys. J. **72**, 97 (1997).
[14] Q. Liu, Y. Wang, W. Guo, H. Ji, J. Xue, and Q. Ouyang, Phys. Rev. E **75**, 051201 (2007).
[15] J. Cervera, B. Schiedt, and P. Ramírez, Europhys. Lett. **71**, 35 (2005).
[16] J. Cervera, B. Schiedt, R. Neumann, S. Mafé, and P. Ramírez, J. Chem. Phys. **124**, 104706 (2006).
[17] H. Daiguji, Y. Oka, and K. Shirono, Nano Lett. **5**, 2274 (2005).
[18] H. Daiguji, P. Yang, and A. Majumdar, Nano Lett. **4**, 137 (2004).
[19] W. Nonner and B. Eisenberg, Biophys. J. **75**, 1287 (1998).
[20] B. Corry, S. Kuyucak, and S. H. Chung, Biophys. J. **78**, 2364 (2000).
[21] D. Boda, M. Valiskó, B. Eisenberg, W. Nonner, D. Henderson, and D. Gillespie, Phys. Rev. Lett. **98**, 168102 (2007).
[22] D. Boda, W. Nonner, M. Valiskó, D. Henderson, B. Eisenberg, and D. Gillespie, Biophys. J. (to be published).
[23] P. Y. Apel, Y. E. Korchev, Z. Siwy, R. Spohr, and M. Yoshida, Nucl. Instrum. Methods Phys. Res. B **184**, 337 (2001).
[24] Z. Siwy, Adv. Funct. Mater. **16**, 735 (2006).
[25] R. Spohr, German Patent No. DE 2951376 C2 (1983); U.S. Patent No. 4,369,370 (1983).
[26] A. Wolf-Reber, Ph.D. thesis (2002).
[27] Z. Grabarek and J. Gergely, Anal. Biochem. **185**, 131 (1990).
[28] H. G. L. Coster, Biophys. J. **5**, 669 (1965).
[29] I. C. Bassignana and H. Reiss, J. Membr. Sci. **15**, 27 (1983).
[30] S. Mafé and P. Ramírez, Acta Polym. **48**, 234 (1997).
[31] Z. Siwy, M. R. Powell, E. Kalman, R. D. Astumian, and R. S. Eisenberg, Nano Lett. **6**, 473 (2006).
[32] Z. Siwy, M. R. Powell, A. Petrov, E. Kalman, C. Trautmann, and R. S. Eisenberg, Nano Lett. **6**, 1729 (2006).
[33] D. Gillespie and R. S. Eisenberg, Phys. Rev. E **63**, 061902 (2001).
[34] L. Shampine, P. Muir, and H. Xu, JNAIAM **1**, 201 (2006).
[35] Z. Siwy and A. Fuliński, Phys. Rev. Lett. **89**, 198103 (2002).
[36] Z. Siwy and A. Fuliński, Am. J. Phys. **72**, 567 (2004).